Temperature-linear resistivity in twisted double bilayer graphene

Yanbang Chu [1,2] Le Liu,[1,2] Cheng Shen,[1,2] Jinpeng Tian [1,2] Jian Tang,[1,2] Yanchong Zhao,[1,2] Jieying Liu [1,2]
Yalong Yuan,[1,2] Yiru Ji,[1,2] Rong Yang,[1,3] Kenji Watanabe [4] Takashi Taniguchi,[5] Dongxia Shi,[1,2,3]
Fengcheng Wu [6,7] Wei Yang [1,2,3,*] and Guangyu Zhang[1,2,3,*]

[1]*Beijing National Laboratory for Condensed Matter Physics, Institute of Physics, Chinese Academy of Sciences, Beijing 100190, China*
[2]*School of Physical Sciences, University of Chinese Academy of Sciences, Beijing 100049, China*
[3]*Songshan Lake Materials Laboratory, Dongguan, Guangdong 523808, China*
[4]*Research Center for Functional Materials, National Institute for Materials Science, 1-1 Namiki, Tsukuba 305-0044, Japan*
[5]*International Center for Materials Nanoarchitectonics, National Institute for Materials Science, 1-1 Namiki, Tsukuba 305-0044, Japan*
[6]*School of Physics and Technology, Wuhan University, Wuhan 430072, China*
[7]*Wuhan Institute of Quantum Technology, Wuhan 430206, China*

We report an experimental study of carrier density (n), displacement field, and twist angle (θ) dependence of temperature (T)-linear resistivity in twisted double-bilayer graphene (TDBG). For a large twist angle ($\theta > 1.5°$) where correlated insulating states are absent, we observe a T-linear resistivity (with a slope on the order of $\sim 10 \, \Omega/K$) over a wide range of carrier densities, and its slope decreases with increasing n, which is in agreement with the acoustic phonon scattering model semiquantitatively. The slope of T-linear resistivity is nonmonotonically dependent on the displacement field with a single peak structure. For a device with $\theta \sim 1.23°$ at which correlated states emerge, the slope of T-linear resistivity is found to be a maximum ($\sim 100 \, \Omega/K$) at the boundary of the halo structure where phase transition occurs, with signatures of continuous phase transition, Planckian dissipation, and diverging effective mass. These observations are in line with quantum critical behaviors, which might be due to symmetry-breaking instability at the critical points. Our results shed new light on correlated physics in TDBG and other twisted moiré systems.

I. INTRODUCTION

Resistivity (ρ) is a measure of how electrons are transported and scattered in solids, and it gives rich and fundamental information of the underlying system. It usually shows a power law dependence on temperature (T), $\rho \propto T^{\alpha}$, where α is an exponent that differs for different scattering mechanisms. Of particular interest is a linear regime where $\alpha = 1$, since it could originate from conventional acoustic phonon couplings [Fig. 1(a)] [1], but also it might indicate unconventional processes that are rooted in quantum criticality [2–4] [Fig. 1(b)]. The latter strange metal behaviors are observed in various correlated systems—for instance, cuprates [5], iron-based compounds [6,7], heavy fermion systems [8,9], Kondo lattices [10], and frustrated lattices [11,12], where quantum critical points are found with the instabilities of order parameters. So far, most previous studies require multiple samples to obtain a single phase diagram, and improved *in situ* sample tunability is demanded.

Moiré superlattices have emerged as a flat band system [13] for realizing a variety of interaction-driven quantum phases [14–19]. Large temperature-linear (T-linear) resistivity has been observed in twisted bilayer graphene (TBG) [20,21], which bears a lot of similarity with that in optimally doped cuprates [22]. While the experiments in Ref. [20] support the electron–phonon scatterings [23,24], those in Ref. [21] raise the possibility of strange metal behavior with near-Planckian dissipation in magic angle TBG, leaving the origin of the T-linear resistivity in TBG still elusive. In twisted double-bilayer graphene (TDBG), observations of halo structures with field-tunable, symmetry-breaking correlated states, as well as T-linear resistivity, have been reported [25–28]. The phase transitions from normal metallic states to correlated states occur at the boundaries of the halo structure in TDBG. Compared to TBG, TDBG is advantageous in tuning electron interactions *in situ* by displacement field. The displacement field changes the flat bandwidth W and superlattice gap Δ in the band structure of TDBG [29], and thus acts as an extra parameter to control the relative strength of electron interactions to kinetic energy. The previous reports mainly focus on the nonlinear regime where ρ rapidly drops at low T, and the linear behaviors at high T are observed yet barely explored, demanding an in-depth and systematic exploration.

In this work, we systematically study T-linear resistivity in TDBG. We found T-linear resistivity in devices with twist angles from 1.23° to 1.91°. First, we study the devices with large twist angles ($\theta > 1.5°$) where correlated insulating states are absent, and find that acoustic phonon scatterings can fully account for the T-linear resistivity. Meanwhile, we also demonstrate a displacement field tunable electron–phonon interaction. Second, in devices with $\theta \sim 1.23°$, we reveal the

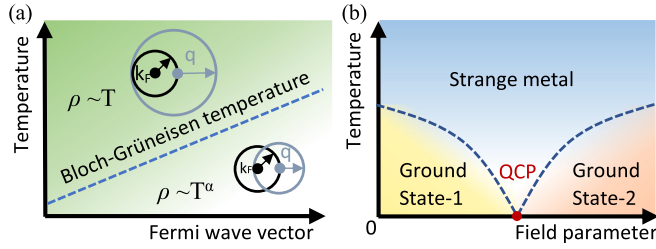*wei.yang@iphy.ac.cn; gyzhang@iphy.ac.cn

FIG. 1. Schematics of T-linear resistivity originated from (a) electron–phonon scattering and (b) the quantum critical point (QCP). The Bloch-Grüneisen temperature (T_{BG}) is defined when Fermi momentum k_F is half of the maximum phonon wave vector q, and $\alpha > 1$ at $T < T_{BG}$.

features beyond the phonon model and discuss the possibility of quantum criticality.

II. T-LINEAR RESISTIVITY AND FIELD-TUNABLE ELECTRON–PHONON COUPLING

The TDBG samples are prepared by a "cut and stack" technique [30–33], and the devices are fabricated with a dual-gate Hall bar geometry in bubble-free region of the samples. The dual-gate geometry enables independent tuning of carrier density (n) and electric displacement field (D), via $n = (C_{BG}V_{BG} + C_{TG}V_{TG})/e$ and $D = (C_{BG}V_{BG} - C_{TG}V_{TG})/2\varepsilon_0$, where $C_{BG}(C_{TG})$ is the geometrical capaci-

tance per area for bottom/top dielectric layer, $V_{BG}(V_{TG})$ is the bottom/top gate voltage, e is the elementary charge, and ε_0 is the vacuum permittivity. Figure 2(a) shows $\rho(n, D)$ at $T = 1.8$ K in a 1.55° device, revealing the charge-neutral point (CNP) and moiré gaps on electron branches ($_+n_s$). The moiré filling factor $v = 4n/n_s$ corresponds to the number of carriers per moiré unit cell, where $n_s = 4/A \approx 8\theta^2/\sqrt{3}a^2$ is the carrier density at full filling and a is the graphene lattice constant.

We first focus on the 1.55° device in Fig. 2, where correlated states are absent at $T = 1.8$ K. Figure 2(b) shows the $\rho(T)$ curves for fillings v from 0.5 to 2.5 at $D = 0$ V/nm. T-linear resistivity with $\rho \propto A_1 T$ is observed at $T > T^*$, indicated by the orange dashed lines in Fig. 2(b). Here, A_1 is the linear slope and T^* is the characteristic temperature that separates the linear regime at $T > T^*$ and the nonlinear regime at $T < T^*$. The A_1 is plotted against n in Fig. 2(c), with values of about 10 to 30 Ω/K, and it decreases as n increases. The onset temperature T^* can be obtained in a quadratic plot ρ–T^2 (see Supplemental Material) [34], and it increases with n as shown in Fig. 2(d).

Our experimental data are captured quantitatively by an electron–phonon scattering model in TDBG [35]. In this model, acoustic phonon scattering [36–39] is enhanced due to a reduced Fermi velocity in TDBG moiré bands, and it predicts a crossover from T at a high temperature to T^4 at a low temperature. If electron–electron Umklapp scattering [40] dominates over phonon scattering at a low temperature, the nonlinear term could become T^2, as shown by the
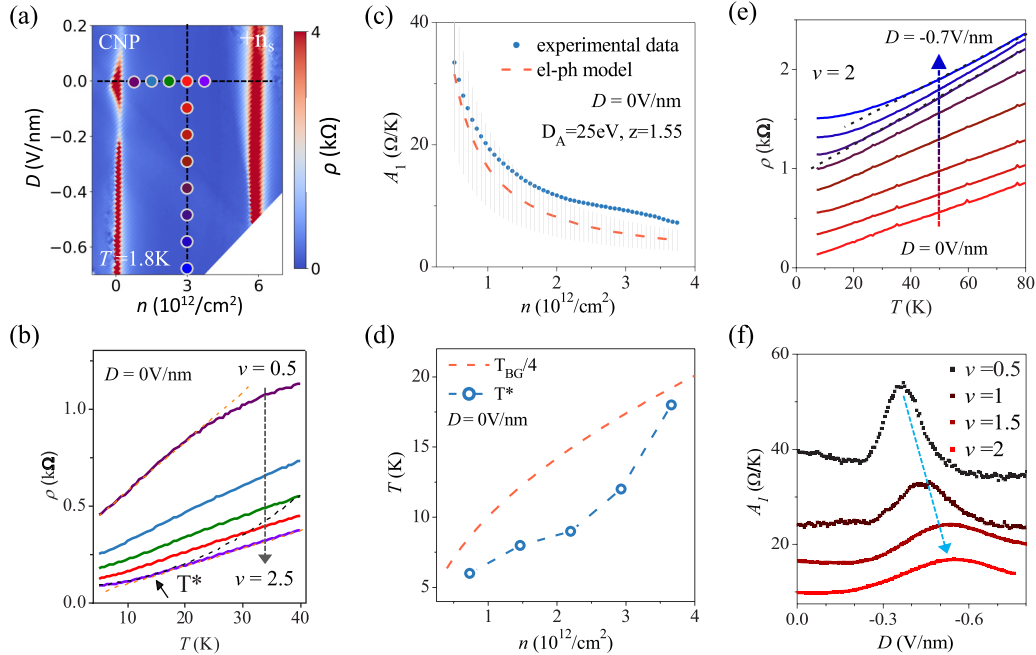

FIG. 2. T-linear resistivity and field-tunable electron (el)–phonon (ph) interactions in 1.55° TDBG. (a) A color mapping of $\rho(n, D)$ at $T = 1.8$ K. (b) $\rho(T)$ at $D = 0$ V/nm for v from 0.5 to 2.5, with a step of 0.5. The black arrow marks the T^*. (c) Experimental $A_1(n)$ at $D = 0$ V/nm (blue dotted line), and phonon model prediction (orange dashed line) with $m^* = 0.15m_e$ calculated from the continuum minimal model. We set the error bar of the simulation to 40%, mainly due to the uncertainty of the acoustic phonon deformation potential and effective mass. (d) One-fourth of theoretical Bloch-Grüneisen temperature ($T_{BG}/4$) and experimental T-linear onset temperature (T^*) for a 1.55° device at $D = 0$ V/nm. (e) $\rho(T)$ at $v = 2$ for D from 0 to -0.7 V/nm, with a step of 0.1 V/nm and offset 200 Ω between curves. The positions of these ρ–T curves in (b) and (e) are marked as colored dots in (a). (f) $A_1(D)$ at $v = 0.5$, 1, 1.5 and 2, with an offset of 5 Ω/K for clarity. The light-blue dashed arrow illustrates the shift of the A_1 peak with decreasing v.
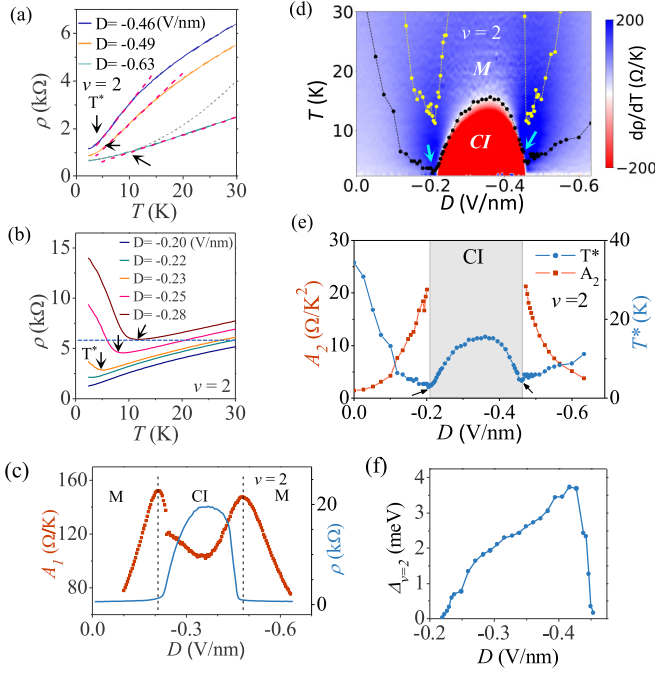
FIG. 3. T-linear resistivity and critical behaviors at the boundaries of halo structures in 1.23° TDBG. (a) Plots of $\rho(T)$ outside the halo at $v = 2$. The dashed line is T^2 dependence-fitted by the experimental curve at $T < T^*$. The pink dashed lines show the T-linear resistivity at $T > T^*$. (b) Plots of $\rho(T)$ near critical points at $v = 2$. (c) Plots of $A_1(D)$ and $\rho(D)$ at $v = 2$, where $\rho(D)$ is measured at $T = 1.8$ K. Here, and "CI" denotes "correlated insulator." (d) A mapping of the numerical $d\rho/dT$ at $v = 2$. T^* is marked by black dots. The upper temperature boundaries of T-linear resistivity are marked by yellow dots. The cyan arrows indicate the critical points. (e) D-dependent A_2 and T^* at $v = 2$. (f) Thermal excitation gap at $v = 2$ as a function of displacement field.

black dashed lines in Fig. 2(b). In the linear regime, the slope A_1 resulting from acoustic phonon scattering [35] is given by

$$A_1 = \frac{\pi D_A^2 k_B z_\infty}{2 g_s g_v e^2 \hbar \rho_m v_{\text{ph}}^2 v_F^2},$$ (1)

where $g_s(g_v)$ are spin (valley) degeneracies, ρ_m is the mass density of graphene, D_A is acoustic phonon deformation potential, v_{ph} and v_F are phonon velocity and Fermi velocity, and z_∞ is the integral concerning phonon occupation and other scattering details in TDBG. We plot the calculated A_1 as a function of n for $\theta = 1.55^\circ$ in Fig. 2(c) (orange dashed line), using $\rho_m = 7.6 \times 10^{-7}$ kg/m², $v_{\text{ph}} = 2.1 \times 10^4$ m/s, $D_A = 25$ eV, $z_\infty = 1.55$ [20,35], and $v_F = \sqrt{(\hbar^2 n\pi/2)}/m^*$, with effective mass $m^* \approx 0.15 m_e$ calculated from the band structure in the continuum minimal model [13,41]. The calculated A_1 and the measured value in Fig. 2(c) are in good agreement. Moreover, the measured T^* matches well with 1/4 of the Bloch-Grüneisen temperature T_{BG} in Fig. 2(d), which further supports the phonon model [35]. Here, T_{BG} is defined as $2\hbar v_{\text{ph}} k_F/k_B$, where $k_F = \sqrt{\pi n/2}$ is the effective Fermi wave vector.
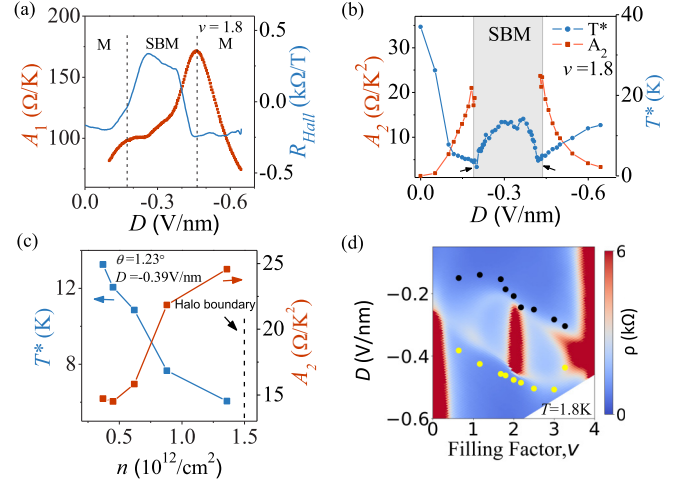
FIG. 4. T-linear resistivity near halo boundaries in 1.23° TDBG. (a) A_1 and Hall coefficient as a function of displacement field. R_{Hall} is measured at $B = 0.1$ T. The vertical dashed lines mark the positions of A_1 peaks, which are located near the abrupt change of R_{Hall}. (b) D-dependent A_2 and T^*. The black arrows indicate the critical points, and the gray areas are the regime of correlated ground states inside the halo "SBM" denotes the "symmetry broken metal." (c) Quadratic temperature dependence of resistivity at constant displacement field in 1.23° TDBG. $T^*(A_2)$ decreases (increases) approaching the halo boundary, consistent with the observation at constant carrier density measurements in Fig. 3. (d) The positions of A_1 peaks for different v in the $\rho(v, D)$ mapping, marked as colored dots.

We also demonstrate that the electron–phonon scatterings are tunable by D field. Figure 2(e) shows the $\rho(T)$ curves at $v = 2$ for different D fields from 0 to –0.7 V/nm in the 1.55° device, with the linear behaviors well preserved. Figure 2(f) presents the curves of extracted A_1 as a function of D at different v, which shows a nonmonotonical dependence with peaks at finite D. Since $A_1 \propto m^{*2}$ at a fixed v, the D-dependent A_1 suggests a field-tunable moiré-band dispersion in TDBG [42]. As indicated by the arrow in Fig. 2(f), the peak position in D shifts with v, demonstrating the electron filling effect on band structure [26,43].

III. ENHANCEMENT OF T-LINEAR RESISTIVITY AT THE HALO BOUNDARY

Next, we turn to the 1.23° device with correlated insulating states and concomitant halo structure in a moiré conduction band. T-linear resistivity with $\rho \sim A_1 T$ is observed at $v = 2$ for $T > T^*$ in Figs. 3(a) and 3(b). Sublinear behaviors at higher temperatures are also observed, which might be due to thermal excitations of remote dispersive bands [20]. The extracted A_1 is plotted against the D field as red dots in Fig. 3(c), and it is strongly field tunable with a large magnitude of $\sim$100 Ω/K. The nonmonotonical dependent $A_1(D)$ shows two peaks with an M-shaped structure in Fig. 3(c), and the peaks are located at the critical point of the metal–insulator transition. The two M-shaped peaks of A_1 are also observed at $v = 1.8$ [Fig. 4(a)] and other fillings (see Supplemental Material Fig. S6) [34]. At $v = 1.8$, the A_1 peaks are found concurrent with a sharp change of Hall coefficient, indicating phase
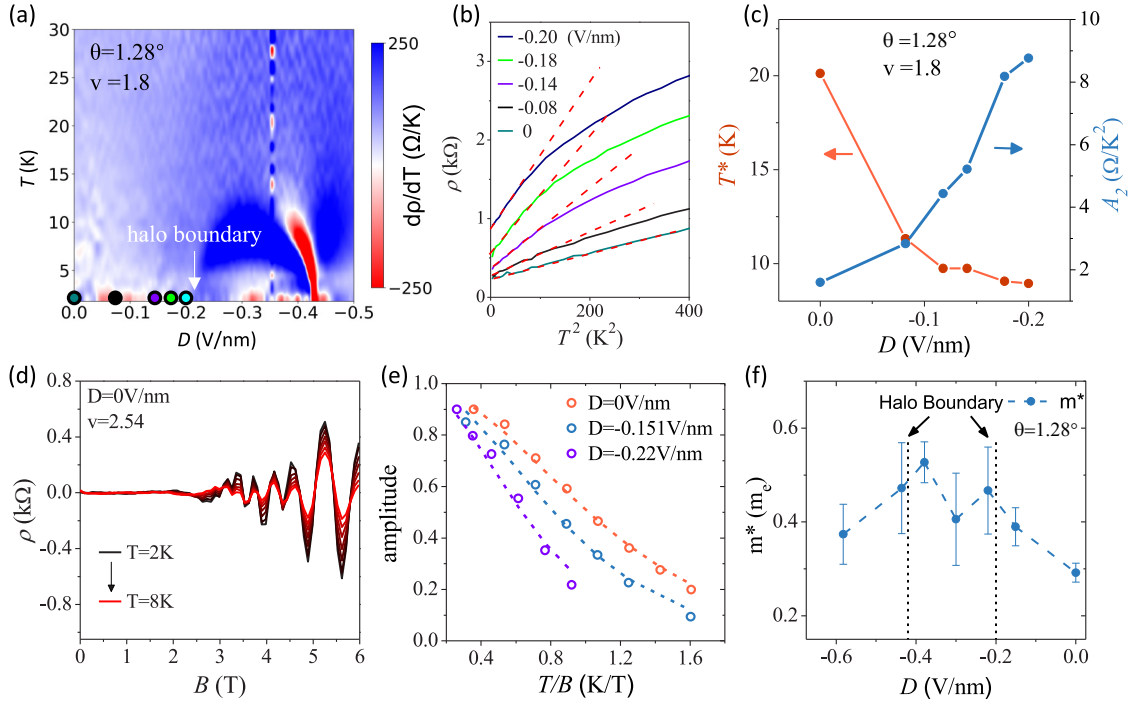
FIG. 5. Quadratic-in-T resistivity in 1.28° TDBG. (a) A color mapping of dρ/dT as a function of displacement field and temperature. (b) Resistivity as a function of T^2 at $v = 1.8$. The positions of the displacement fields are marked by colored dots in (a). The red dashed lines show the increasing A_2 as it approaches the boundary of the halo. (c) The field dependence of T^* and A_2 extracted from ρ–T^2 plots in (b). (d) Temperature-dependent Shubnikov de Haas (SdH) oscillation amplitude. (e) Normalized oscillation amplitude as a function of T/B at representative displacement fields. (f) Extracted effective mass at different displacement fields.

transitions between metallic phases with broken symmetry and those without [28]. Moreover, these A_1 peaks are found following the boundary of the halo structure in Fig. 4(d), implying the correlation between the enhancement of A_1 and phase transitions. From the phonon model, the increase of A_1 at the halo boundary suggests the enhancement of effective mass.

To reveal the effective mass better, we analyze the temperature dependence of resistivity at $T < T^*$. For the metals outside the halo structure, we observe signatures of quadratic resistivity $\rho \sim A_2 T^2$ at $T < T^*$, as shown in Fig. 3(a). The D-dependent T^* and A_2 are plotted in Figs. 3(d) and 3(e). We find a decreasing T^* and an increasing A_2 when approaching the critical displacement field. The quadratic power law at low temperature indicates Landau Fermi liquid behavior, in which $A_2 \propto \frac{k_F}{E_F^2} \propto \frac{m^{*}\alpha}{n^\beta}$, with α and β being the exponents that depend on the details of band structure [44]. It is worth noting that the $A_2(D)$ also qualitatively agrees with the $A_1(D)$ in the phonon scatterings model, since $A_1 \propto 1/v_F^2 \propto m^{*2}/n$. The increased m^* at the halo boundary is also revealed in the carrier density–dependent $A_2(n)$ at a fixed D [Fig. 4(c)]. Such quadratic dependence of resistivity is also well reproduced from another TDBG device with $\theta = 1.28°$ in Figs. 5(a) and 5(b), and the corresponding field-dependent A_2 also tends to diverge at the halo boundary in Fig. 5(c), similar to those observations in Fig. 4. For reference, direct measurement of m^* by the Lifshitz-Kosevich method is also carried out for the 1.28° device in Figs. 5(d)–5(f).

IV. DICUSSION OF POSSIBLE QUANTUM CRITICAL BEHAVIOR

One important question is why the m^* tends to diverge at the boundaries of the halo structure. Though the change of m^* could explain the change of A_1 and A_2 based on the electron–phonon scattering model and Fermi liquid scenario, the observation of diverging m^* is unusual by itself, and it may call for the possibility of quantum criticality. Given the correlation between diverging m^* and symmetry-breaking phase transition at the critical points of the halo structure, the diverging m^* suggests the possible existence of quantum critical behaviors [45,46], which we discuss next. First, the phase transitions at the critical points of the halo structure are continuous in the temperature range we studied, indicated by the vanishing thermal activation gap [Fig. 3(f)]. Second, the decreasing T^* and the increasing A_2 when approaching the critical displacement field outside the halo structure in Fig. 3(d) and Fig. 4(b) are also signatures of quantum critical behaviors [45]. Last, we find the large T-linear resistivity falls into the Planckian dissipation regime where the scattering rate is proportional to temperature, $\hbar/\tau = Ck_BT$ and the coefficient C approaches $O(1)$. In a graphene moiré system [21], the number C can be extracted from T-linear resistivity slope A_1 by $C = \hbar e^2 n A_1/k_B m^*$. In our cases, we obtain $C \sim 1.8$ for the A_1 peaks at $v = 2$ in Fig. 3(c) by taking $m^* = 0.3 \, m_e$, $n = 1.75 \times 10^{12}/\text{cm}^2$, and $A_1 = 146 \, \Omega/\text{K}$. All these facts suggest the possible existence of quantum criticality at the boundaries of the halo structure.

At continuous phase transition critical points, quantum fluctuations associated with symmetry-breaking order parameters can be significant. In TDBG, the boundary of the halo structure separates states with different symmetry, which is likely to generate quantum fluctuations. More specifically, we suspect it is the spin fluctuations [47] that contribute to the T-linear resistivity. While spin-up electrons and spin-down electrons are equally filled outside the halo, one is more favored than the other inside the halo structure [26]. However, more experimental and theoretical investigations are required for a better understanding.

V. CONCLUSION

In conclusion, we systematically investigate the carrier density, displacement field, and twist angle dependences of T-linear resistivity in TDBG. We demonstrate a dominant role played by acoustic phonons when correlated states are absent at $\theta > 1.5°$. The T-linear resistivity has a nonmonotonic displacement field dependence with a single A_1 peak, revealing the field-tunable electron–phonon interaction in TDBG. Moreover, we observe an M-shaped two-peak structure in the presence of correlated states at $\theta \sim 1.23°$. These peaks are located at the halo boundary, separating states with different symmetries. We propose the possible existence of quantum criticality, supported by the evidence of continuous phase transition, vanishing T^*, Planckian dissipation, and the diverging effective mass at the critical points. Our observations establish a close link between high temperature T-linear resistivity and low-temperature ground states, and hopefully inspire more work about the nature of quantum criticality and ground-state instability in TDBG [48]. Similar phenomena may also be expected in other field-tunable systems such as twisted monolayer–bilayer graphene [49–51] and an rhombohedral trilayer graphene/hexagonal boron nitride moiré system [52].

[1] J. M. Ziman, *Electrons and Phonons: The Theory of Transport Phenomena in Solids* (Oxford University Press, Oxford, 2001).

[2] C. M. Varma, Colloquium: Linear in temperature resistivity and associated mysteries including high temperature superconductivity, Rev. Mod. Phys. **92**, 031001 (2020).

[3] P. Coleman and A. J. Schofield, Quantum criticality, Nature (London) **433**, 226 (2005).

[4] S. Sachdev and B. Keimer, Quantum criticality, Phys. Today **64**(2), 29 (2011).

[5] B. Keimer, S. A. Kivelson, M. R. Norman, S. Uchida, and J. Zaanen, From quantum matter to high-temperature superconductivity in copper oxides, Nature (London) **518**, 179 (2015).

[6] T. Shibauchi, A. Carrington, and Y. Matsuda, A quantum critical point lying beneath the superconducting dome in iron pnictides, Annu. Rev. Condens. Matter Phys. **5**, 113 (2014).

[7] R. Zhou, Z. Li, J. Yang, D. L. Sun, C. T. Lin, and G.-Q. Zheng, Quantum criticality in electron-doped Ba Fe$_{2-x}$Ni$_x$As$_2$, Nat. Commun. **4**, 2265 (2013).

[8] P. Gegenwart, Q. Si, and F. Steglich, Quantum criticality in heavy-fermion metals, Nat. Phys. **4**, 186 (2008).

[9] G. Stewart, Non-Fermi-liquid behavior in d- and f-electron metals, Rev. Mod. Phys. **73**, 797 (2001).

[10] B. Shen, Y. Zhang, Y. Komijani, M. Nicklas, R. Borth, A. Wang, Y. Chen, Z. Nie, R. Li, X. Lu, H. Lee, M. Smidman, F. Steglich, P. Coleman, and H. Yuan, Strange-metal behaviour in a pure ferromagnetic Kondo lattice, Nature (London) **579**, 51 (2020).

[11] L. Cano-Cortes, J. Merino, and S. Fratini, Quantum Critical Behavior of Electrons at the Edge of Charge Order, Phys. Rev. Lett. **105**, 036405 (2010).

[12] T. Sato, K. Kitai, K. Miyagawa, M. Tamura, A. Ueda, H. Mori, and K. Kanoda, Strange metal from a frustration-driven charge order instability, Nat. Mater. **18**, 229 (2019).

[13] R. Bistritzer and A. H. MacDonald, Moiré bands in twisted double-layer graphene, Proc. Natl. Acad. Sci. USA **108**, 12233 (2011).

[14] Y. Cao, V. Fatemi, A. Demir, S. Fang, S. L. Tomarken, J. Y. Luo, J. D. Sanchez-Yamagishi, K. Watanabe, T. Taniguchi, E. Kaxiras, R. C. Ashoori, and P. Jarillo-Herrero, Correlated insulator behaviour at half-filling in magic-angle graphene superlattices, Nature (London) **556**, 80 (2018).

[15] Y. Cao, V. Fatemi, S. Fang, K. Watanabe, T. Taniguchi, E. Kaxiras, and P. Jarillo-Herrero, Unconventional superconductivity in magic-angle graphene superlattices, Nature (London) **556**, 43 (2018).

[16] M. Yankowitz, S. Chen, H. Polshyn, Y. Zhang, K. Watanabe, T. Taniguchi, D. Graf, A. F. Young, and C. R. Dean, Tuning superconductivity in twisted bilayer graphene, Science **363**, 1059 (2019).

[17] X. Lu, P. Stepanov, W. Yang, M. Xie, M. A. Aamir, I. Das, C. Urgell, K. Watanabe, T. Taniguchi, G. Zhang, A. Bachtold, A. H. MacDonald, and D. K. Efetov, Superconductors, orbital magnets and correlated states in magic-angle bilayer graphene, Nature (London) **574**, 653 (2019).

[18] A. L. Sharpe, E. J. Fox, A. W. Barnard, J. Finney, K. Watanabe, T. Taniguchi, M. A. Kastner, and D. Goldhaber-Gordon, Emergent ferromagnetism near three-quarters filling in twisted bilayer graphene, Science **365**, 605 (2019).

[19] M. Serlin, C. L. Tschirhart, H. Polshyn, Y. Zhang, J. Zhu, K. Watanabe, T. Taniguchi, L. Balents, and A. F. Young, Intrinsic quantized anomalous Hall effect in a moiré heterostructure, Science **367**, 900 (2020).

[20] H. Polshyn, M. Yankowitz, S. Chen, Y. Zhang, K. Watanabe, T. Taniguchi, C. R. Dean, and A. F. Young, Large linear-in-temperature resistivity in twisted bilayer graphene, Nat. Phys. **15**, 1011 (2019).

[21] Y. Cao, D. Chowdhury, D. Rodan-Legrain, O. Rubies-Bigorda, K. Watanabe, T. Taniguchi, T. Senthil, and P. Jarillo-Herrero, Strange Metal in Magic-Angle Graphene with Near Planckian Dissipation, Phys. Rev. Lett. **124**, 076801 (2020).

[22] J. A. N. Bruin, H. Sakai, R. S. Perry, and A. P. Mackenzie, Similarity of scattering rates in metals showing T-linear resistivity, Science **339**, 804 (2013).

[23] F. Wu, E. Hwang, and S. Das Sarma, Phonon-induced giant linear-in-T resistivity in magic angle twisted bilayer graphene: Ordinary strangeness and exotic superconductivity, Phys. Rev. B **99**, 165112 (2019).

[24] G. Sharma, I. Yudhistira, N. Chakraborty, D. Y. H. Ho, M. M. A. Ezzi, M. S. Fuhrer, G. Vignale, and S. Adam, Carrier transport theory for twisted bilayer graphene in the metallic regime, Nat. Commun. **12**, 5737 (2021).

[25] Y. Cao, D. Rodan-Legrain, O. Rubies-Bigorda, J. M. Park, K. Watanabe, T. Taniguchi, and P. Jarillo-Herrero, Tunable correlated states and spin-polarized phases in twisted bilayer–bilayer graphene, Nature (London) **583**, 215 (2020).

[26] X. Liu, Z. Hao, E. Khalaf, J. Y. Lee, Y. Ronen, H. Yoo, D. H. Najafabadi, K. Watanabe, T. Taniguchi, A. Vishwanath, and P. Kim, Tunable spin-polarized correlated states in twisted double bilayer graphene, Nature (London) **583**, 221 (2020).

[27] C. Shen, Y. Chu, Q. Wu, N. Li, S. Wang, Y. Zhao, J. Tang, J. Liu, J. Tian, K. Watanabe, T. Taniguchi, R. Yang, Z. Y. Meng, D. Shi, O. V. Yazyev, and G. Zhang, Correlated states in twisted double bilayer graphene, Nat. Phys. **16**, 520 (2020).

[28] M. He, Y. Li, J. Cai, Y. Liu, K. Watanabe, T. Taniguchi, X. Xu, and M. Yankowitz, Symmetry breaking in twisted double bilayer graphene, Nat. Phys. **17**, 26 (2020).

[29] G. W. Burg, J. Zhu, T. Taniguchi, K. Watanabe, A. H. MacDonald, and E. Tutuc, Correlated Insulating States in Twisted Double Bilayer Graphene, Phys. Rev. Lett. **123**, 197702 (2019).

[30] Y. Saito, J. Ge, K. Watanabe, T. Taniguchi, and A. F. Young, Independent superconductors and correlated insulators in twisted bilayer graphene, Nat. Phys. **16**, 926 (2020).

[31] K. Kim, M. Yankowitz, B. Fallahazad, S. Kang, H. C. P. Movva, S. Huang, S. Larentis, C. M. Corbet, T. Taniguchi, K. Watanabe, S. K. Banerjee, B. J. LeRoy, and E. Tutuc, Van der Waals heterostructures with high accuracy rotational alignment, Nano Lett. **16**, 1989 (2016).

[32] Y. Cao, J. Y. Luo, V. Fatemi, S. Fang, J. D. Sanchez-Yamagishi, K. Watanabe, T. Taniguchi, E. Kaxiras, and P. Jarillo-Herrero, Superlattice-Induced Insulating States and Valley-Protected Orbits in Twisted Bilayer Graphene, Phys. Rev. Lett. **117**, 116804 (2016).

[33] K. Kim, A. DaSilva, S. Huang, B. Fallahazad, S. Larentis, T. Taniguchi, K. Watanabe, B. J. LeRoy, A. H. MacDonald, and E. Tutuc, Tunable moiré bands and strong correlations in small-twist-angle bilayer graphene, Proc. Natl. Acad. Sci. USA **114**, 3364 (2017).

[34] See Supplemental Material at http://link.aps.org/supplemental/10.1103/PhysRevB.106.035107 for a discussion of quadratic-in-T resistivity at low temperature and enhanced T-linear resistivity near the halo boundary.

[35] X. Li, F. Wu, and S. Das Sarma, Phonon scattering induced carrier resistivity in twisted double-bilayer graphene, Phys. Rev. B **101**, 245436 (2020).

[36] A. C. Betz, S. H. Jhang, E. Pallecchi, R. Ferreira, G. Fève, J. M. Berroir, and B. Plaçais, Supercollision cooling in undoped graphene, Nat. Phys. **9**, 109 (2012).

[37] D. K. Efetov and P. Kim, Controlling Electron-Phonon Interactions in Graphene at Ultrahigh Carrier Densities, Phys. Rev. Lett. **105**, 256805 (2010).

[38] J. C. Song, M. Y. Reizer, and L. S. Levitov, Disorder-Assisted Electron-Phonon Scattering and Cooling Pathways in Graphene, Phys. Rev. Lett. **109**, 106602 (2012).

[39] E. H. Hwang and S. Das Sarma, Acoustic phonon scattering limited carrier mobility in two-dimensional extrinsic graphene, Phys. Rev. B **77**, 115449 (2008).

[40] J. R. Wallbank, R. Krishna Kumar, M. Holwill, Z. Wang, G. H. Auton, J. Birkbeck, A. Mishchenko, L. A. Ponomarenko, K. Watanabe, T. Taniguchi, K. S. Novoselov, I. L. Aleiner, A. K. Geim, and V. I. Fal'ko, Excess resistivity in graphene superlattices caused by Umklapp electron–electron scattering, Nat. Phys. **15**, 32 (2018).

[41] M. Koshino, Band structure and topological properties of twisted double bilayer graphene, Phys. Rev. B **99**, 235406 (2019).

[42] F. Haddadi, Q. Wu, A. J. Kruchkov, and O. V. Yazyev, Moiré flat bands in twisted double bilayer graphene, Nano Lett. **20**, 2410 (2020).

[43] F. Wu and S. Das Sarma, Ferromagnetism and superconductivity in twisted double bilayer graphene, Phys. Rev. B **101**, 155149 (2020).

[44] X. Lin, B. Fauqué, and K. Behnia, Scalable T^2 resistivity in a small single-component Fermi surface, Science **349**, 945 (2015).

[45] S. Licciardello, J. Buhot, J. Lu, J. Ayres, S. Kasahara, Y. Matsuda, T. Shibauchi, and N. E. Hussey, Electrical resistivity across a nematic quantum critical point, Nature (London) **567**, 213 (2019).

[46] J. Custers, P. Gegenwart, H. Wilhelm, K. Neumaier, Y. Tokiwa, O. Trovarelli, C. Geibel, F. Steglich, C. Pépin, and P. Coleman, The break-up of heavy electrons at a quantum critical point, Nature (London) **424**, 524 (2003).

[47] T. Moriya and K. Ueda, Spin fluctuations and high temperature superconductivity, Adv. Phys. **49**, 555 (2000).

[48] L. Liu, S. Zhang, Y. Chu, C. Shen, Y. Huang, Y. Yuan, J. Tian, J. Tang, Y. Ji, R. Yang, K. Watanabe, T. Taniguchi, D. Shi, J. Liu, W. Yang, and G. Zhang, Isospin competitions and

valley polarized correlated insulators in twisted double bilayer graphene, Nat. Commun. **13**, 3292 (2022).

[49] S. Chen, M. He, Y.- H. Zhang, V. Hsieh, Z. Fei, K. Watanabe, T. Taniguchi, D. H. Cobden, X. Xu, C. R. Dean, and M. Yankowitz, Electrically tunable correlated and topological states in twisted monolayer–bilayer graphene, Nat. Phys. **17**, 374 (2020).

[50] H. Polshyn, J. Zhu, M. A. Kumar, Y. Zhang, F. Yang, C. L. Tschirhart, M. Serlin, K. Watanabe, T. Taniguchi, A. H. MacDonald, and A. F. Young, Electrical switching of magnetic order in an orbital Chern insulator, Nature (London) **588**, 66 (2020).

[51] S. Xu, M. M. Al Ezzi, N. Balakrishnan, A. Garcia-Ruiz, B. Tsim, C. Mullan, J. Barrier, N. Xin, B. A. Piot, T. Taniguchi, K. Watanabe, A. Carvalho, A. Mishchenko, A. K. Geim, V. I. Fal'ko, S. Adam, A. H. C. Neto, K. S. Novoselov, and Y. Shi, Tunable Van Hove singularities and correlated states in twisted monolayer–bilayer graphene, Nat. Phys. **17**, 619 (2021).

[52] G. Chen, L. Jiang, S. Wu, B. Lyu, H. Li, B. L. Chittari, K. Watanabe, T. Taniguchi, Z. Shi, J. Jung, Y. Zhang, and F. Wang, Evidence of a gate-tunable Mott insulator in a trilayer graphene moiré superlattice, Nat. Phys. **15**, 237 (2019).